Distinct magnetism in ultrathin epitaxial NiFe$_2$O$_4$ films on MgAl$_2$O$_4$ and SrTiO$_3$ single crystalline substrates

Michael Foerster,[1] José Manuel Rebled,[1,2] Sònia Estradé,[2,3] Florencio Sánchez,[1] Francesca Peiró,[2] and Josep Fontcuberta[1]

[1]*Institut de Ciència de Materials de Barcelona (ICMAB-CSIC), Campus UAB, Bellaterra 08193, Spain*
[2]*LENS – MIND/IN2UB, Departament d'Electrònica, Universitat de Barcelona, c/Martí Franquès 1, Barcelona ES-08028, Spain*
[3]*TEM-MAT, CCiT, Universitat de Barcelona, Solé i Sabarís 1, ES-08028 Barcelona, Spain.*

Spinel ferrites are being considered for advanced spintronic applications. Here, we report on the magnetic properties of ultrathin (3–37 nm) epitaxial films of NiFe$_2$O$_4$ (NFO) on MgAl$_2$O$_4$ (MAO) and SrTiO$_3$ (STO) single crystalline substrates. It is found that NFO films on STO display superparamagnetic response down to 50 K, whereas films grown on MAO display ferrimagnetic response up to room temperature. Microstructural information indicates that this distinct response can be attributed to the different growth mechanisms of the spinel ferrite on the isostructural MAO substrate (two-dimensional growth) and the perovskite STO (Volmer-Weber three-dimensional growth). We discuss the reasons for this distinct behavior and its relevance for the integration of ferrites in epitaxial heterostructures for tunnel devices.

PACS number(s): 75.70.Ak, 75.50.Gg, 68.55.A−, 85.75.−d

I. INTRODUCTION

Ferrimagnetic spinels (AB$_2$O$_4$), such as CoFe$_2$O$_4$, NiFe$_2$O$_4$, or Fe$_3$O$_4$ are receiving renewed attention due to their potential advantageous use in spintronics.[1–3] In some applications, such as in tunnel junctions, epitaxial layers only a few nanometers thick are required and thus detailed understanding of their magnetic and transport properties at such scale is needed. The magnetic order in spinel ferrites is dominated by the strong antiferromagnetic superexchange coupling (J_{AB}) between the tetrahedral A cations and octahedral B cations, giving rise to an uncompensated antiferromagnetic ordering between the ferromagnetically ordered A and B sublattices and thus to a net magnetization moment. This simple picture, proposed by Néel[4] and successfully used to rationalize the magnetic properties of bulk spinels, comes to difficulties when attempting to describe the properties of ultrathin spinel layers.

Indeed, the magnetic properties of thin films of spinels are found to differ from their bulk counterparts and it has been claimed that these differences arise due to surface and interface effects,[5] nonequilibrium cationic distribution,[6] enhanced surface anisotropy,[7] or the formation of antiphase boundaries (APBs).[8,9] APBs are predicted to be formed at the interface between coalescing AB$_2$O$_4$ nuclei; the presence of APBs originates the prevalence of new strong 180° antiferromagnetic interactions M(B)-O-M(B) (where M is a magnetic ion at B sites) across the APBs that do not occur within the spinel domains. A primary consequence of the existence of these antiferromagnetic APBs is that they reduce the magnetization and increase the saturation field as experimentally observed in Fe$_3$O$_4$ (Refs. 9 and 10). Another effect of major consequences for spintronic applications is that the occurrence of APBs may magnetically decouple ferrimagnetic AB$_2$O$_4$ crystallites thus producing a superparamagnetic (SP) behavior in ultrathin films. In fact, SP response at room temperature has been observed in MBE-grown 1.8–5.3 nm thick Fe$_3$O$_4$ films and it was argued to be the consequence of the existence of APBs and a concomitant 180° Fe(B)-O-Fe(B) antiferromagnetic interaction.[9] This observation is of major relevance because a

SP response will cancel expectations for spinels in nanometric tunnel heterostructures. To what extent this phenomenology is shared by other ferrimagnetic spinels and/or it can be modified by appropriate tailoring of the growth mechanism are questions that remain to be settled.

Here, we address these issues by reporting on the magnetic characterization of nanometric thin films of NiFe$_2$O$_4$ (NFO) grown on MgAl$_2$O$_4$ (MAO) and SrTiO$_3$ (STO) single crystalline substrates. NiFe$_2$O$_4$, in contrast to Fe$_3$O$_4$, is a ferrimagnetic insulator ($T_C = 850$ K) of potential use as barrier in spin filters[2,11,12] and thus understanding and controlling its properties in ultrathin films is needed for further integration. The selected cubic substrates differ not only in the matching of the cubic cell parameter a with respect to the NFO ($a_{NFO} = 0.8339$ nm, $a_{MAO} = 0.8083$ nm, and $2a_{STO} = 0.7810$ nm) but also in the atomic stacking and symmetry. While in STO the building blocks are BO$_6$ polyhedra, MAO, being isostructural with NFO, is formed by a chessboard stacking along the three principal directions of cubic cages containing BO$_6$ and AO$_4$ polyhedra. These structural differences are expected to produce significant changes in the magnetic properties of NFO films when grown on STO or MAO and their comparison may provide clues for new understanding.

When growing ultrathin films, we encountered that films grown on MAO seemed to display an enhanced magnetization, similar to that reported earlier for Fe$_3$O$_4$ on MgO (see Ref. 5) or NFO on STO (see Ref. 6). However, we will show that this result is due to the presence of a paramagnetic spurious signal found to be common to all used MAO substrates which becomes prominent at small NFO thicknesses. After correction of such signal, we still observed a significant influence of the substrate (STO or MAO) on the magnetic properties of the NFO thin film. First, the low-temperature magnetization of films deposited on spinel MAO is clearly larger than that of similar films grown on the perovskite STO substrate. Second, even the thinnest (3 nm) NFO films on MAO display a well-behaved ferrimagnetic response with a robust remanence up to room temperature. In contrast, ultrathin (3nm) NFO films on STO clearly show a SP response down

to 50 K with null magnetic remanence. On the basis of high-resolution electron microscopy (HREM) data we argue that these effects result from distinct growth mechanisms on both substrates and chemical interdiffusion from the substrate into the spinel film grown on STO. These observations, casting doubts on the potential of spinel-based thin films on perovskite platforms (substrates, buffer layers or bottom electrodes) for room-temperature operation, provide a microscopic plausible explanation for the rather moderate performance of spinel-based spintronic devices.

II. EXPERIMENTAL

NFO thin films with thickness between 3 and 37 nm were grown simultaneously on MAO (001) and STO (001) substrates by pulsed laser deposition (PLD) from a stochiometric target. The deposition conditions were: substrate temperature $T = 500\,^\circ$C and oxygen pressure $P_{O2} = 0.1$ mbar. A KrF laser with fluence $F = 1.6$ J/cm^2 and a repetition rate of 5 Hz was used. X-ray diffraction (XRD) shows that the films are fully textured and no impurity phases can be detected in $\theta/2\theta$ scans. While both substrates induce in-plane compressive stress [mismatch $(a_{NFO} - a_{MAO})/a_{NFO} \approx 3\%$ for MAO and 6% for STO, respectively], only samples on MAO show a considerable out-of-plane strain of $(a_{NFO,film} - a_{NFO,bulk})/a_{NFO,bulk} \approx 2.2\%$ (for 37 nm thickness) while the equivalent sample on STO is almost fully relaxed (0.3% out-of-plane strain).

Magnetic measurements in the temperature range between 2 and 300 K were performed in a Quantum Design SQUID magnetometer with the magnetic field applied parallel to the film surface after carefully removing any impurity (e.g. silver paste from the deposition process) from the samples sides and backside.

Samples for transmission electron microscopy (TEM) observations were prepared through conventional mechanical polishing for both planar view and cross section orientations. They were observed in a Jeol J2010F scanning TEM (STEM) microscope, with a hot field emission gun at 200 keV, coupled with a GIF spectrometer, which has been used for electron energy loss spectroscopy (EELS) analysis. A Jeol 2100 with a LaB$_6$ filament was used for real diffraction experiments.

III. RESULTS

A. Magnetic characterization

In Fig. 1(a), we show the raw field-dependent magnetic moment *m(H)* measured at 300 K and low temperatures (10 and 5 K) for two pairs of films of different thicknesses: NFO(24)//STO and NFO(24)//MAO as well as NFO(3)//STO and NFO(3)//MAO. The dominating diamagnetic contribution of the substrates, for most of the field range, can be clearly appreciated. At any temperature, the ferrimagnetic contribution is only visible at small fields (<10 kOe). Subtraction of the substrate contribution is necessary to reveal the film contribution. Before stepping into such subtraction, it is worth to notice some features in the raw *m(H)* data of Fig. 1(a): (i) the diamagnetic contribution of MAO is larger than that of STO substrates and, more importantly, the former seems to vary considerably with temperature. (ii) The observation of a smaller negative slope in MAO at low temperature suggests
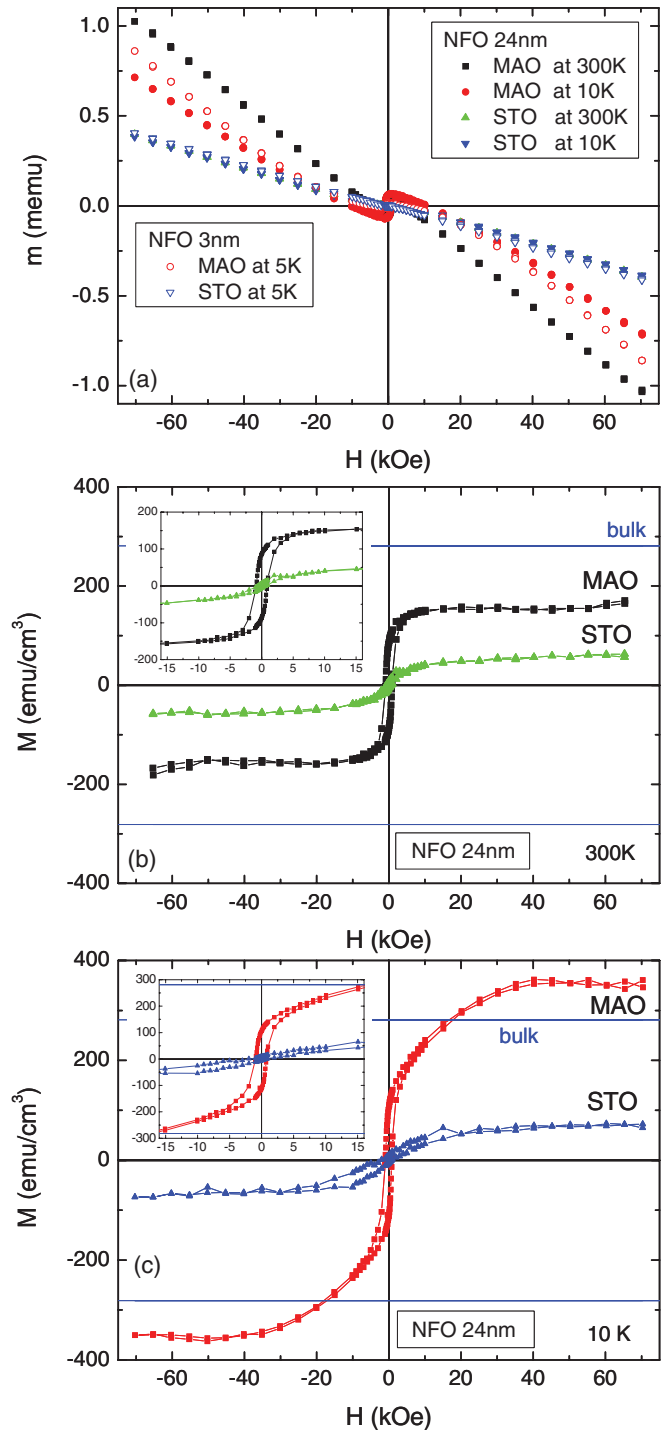

FIG. 1. (Color online) (a) Illustrative *m(H)* raw data for different samples and temperatures as indicated. (b) *M(H)* of 24 nm thick NFO layers after diamagnetic background subtraction at 300 K and (c) at 10 K. Insets: zoom of the low-field region.

the presence of a superimposed paramagnetic contribution (see below).

The magnetic contribution of the substrate $m_{sub}(H)$ is commonly evaluated by fitting the high-field *m(H)* data to a straight line. Subsequently, this line is subtracted from the raw *m(H)* data to obtain the film magnetic moment and so its

magnetization $M(H) = [m(H) - m_{sub}(H)]/V$, where V is the film volume.

Using this approach, the magnetization loops $M(H)$ of the relatively thick (24 nm) NFO film on MAO and STO substrates are evaluated and shown in Figs. 1(b) and 1(c), at 300 and 10 K respectively. Insets in Figs. 1(b) and 1(c) are zooms of the low-field region of the corresponding $M(H)$ loops. Inspection of the room-temperature data [see Fig. 1(b)] shows that (i) after subtraction of the substrate contribution, the $M(H)$ loops appear to be almost saturated at about ∼10 kOe [see inset in Fig. 1(b)], (ii) the magnetization of films grown on MAO is larger than that of films grown on STO, (iii) both films have magnetization values smaller than bulk (line), and (iv) films on MAO display a clear remanence, which is not visible in films on STO (see also below).

The low-temperature $M(H)$ loops shown in Fig. 1(c), display a different behavior: on one side again the magnetization of films grown on STO is smaller than bulk NFO values [line in Fig. 1(c)] and similar to its room-temperature value of Fig. 1(b). On the other side, the $M(H)$ loop of the film on MAO does not appear to be saturated up to ∼40 kOe and reaches magnetization values much larger than at room temperature [see Fig. 1(b)] and substantially larger than bulk. This last observation is in line with earlier reports.[13] However, the magnetization loop of NFO(24)//MAO in Fig. 1(c) displays a nonhomogeneous shape which may signal the presence of distinct contributions to $M(H)$, recalling the observation [see Fig. 1(a)] of a possible paramagnetic contribution arising from the MAO substrate.

To confirm the presence and relevance of a paramagnetic contribution coming from MAO substrates, a thicker (37 nm) NFO film on MAO has been measured at lower temperatures, (8, 5, and 2 K) and compared to $M(H, 5 K)$ data taken for NFO powder obtained directly from the PLD target [see Fig. 2(a)]. A bare MAO substrate from the very same batch was also measured [see Fig. 2(b)]. Notice in Fig. 2(a) that the magnetization values, determined by subtracting a linear contribution due to substrate, largely exceed the bulk value of NFO. Additionally, the very same [NFO(37)//MAO] sample has been annealed at 700 °C in air for 5 h and the $M(H)$ data recorded again at 5 K. It can be appreciated in Fig. 2(a) (crosses) that the magnetization of the film has not changed after this annealing process, thus ruling out that the enhanced magnetization could be related to some nonequilibrium cationic distributions affected by the annealing. More important, the data in Fig. 2(a) show that the $M(H)$ loops of the NFO(37)//MAO sample display features already observed in NFO(24)//MAO [see Fig. 1(c)], namely, an enhanced magnetization and a double-step that gets more pronounced when lowering the temperature. This observation clearly supports the suggested presence of a paramagnetic contribution. In Fig. 2(b), we show the $m(H)$ loop of a MAO substrate recorded at 5 K. This $m(H)$ loop evidences the presence of a paramagnetic component superimposed to a genuine diamagnetic contribution, the former made more evident by (i) plotting the magnetic moment after subtracting the diamagnetic (high-field) contribution as shown in the upper right inset in Fig. 2(b) or by measuring the temperature dependence of the magnetic susceptibility [see Fig 2(b), lower inset]. After subtracting a constant diamagnetic contribution, a clear Curie's law behavior of the inverse susceptibility is
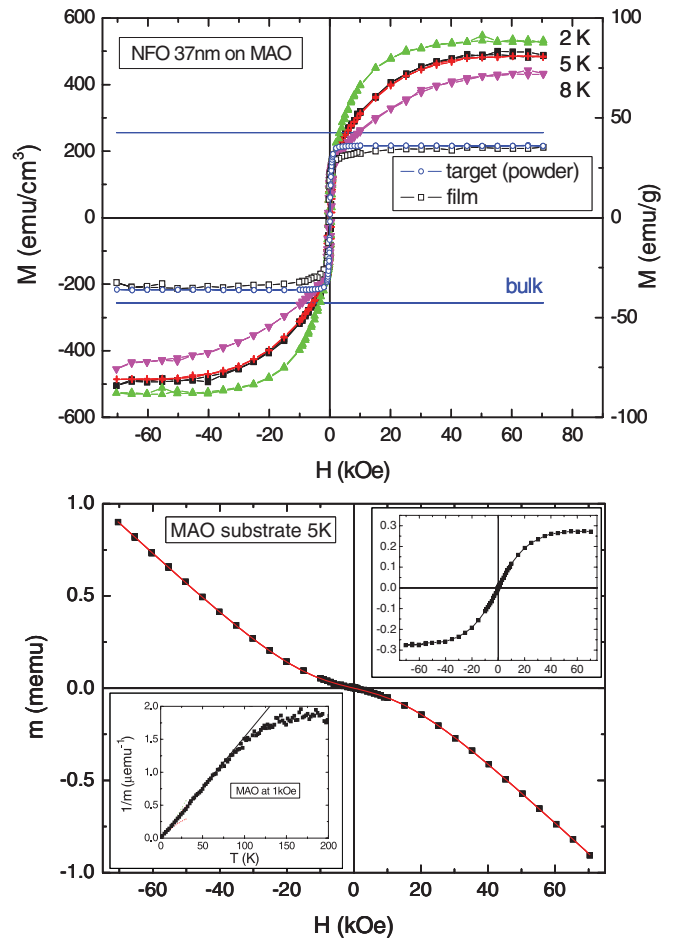

FIG. 2. (Color online) (a) $M(H)$ data of a 37 nm NFO layer on MAO after linear subtraction at different temperatures (2, 5, and 8 K). Solid squares and crosses correspond to data collected at 5 K before and after annealing as described in text. For comparison, data of NFO powder obtained from the PLD target, and a curve obtained by subtracting the MAO substrate [in (b)] is also shown. (b) $m(H)$ measured for a MAO substrate (main panel, the red line is a fit as discussed in Appendix); the resulting $m(H)$ curve after linear subtraction of the diamagnetic contribution is shown in upper inset. Lower inset: inverse susceptibility of the substrate after subtraction of the diamagnetic contribution as function of temperature, showing paramagnetic (Curie's law) behavior.

observed, thus confirming the paramagnetic nature of the spurious contribution arising from the MAO substrate (a quantitative analysis of the MAO substrate magnetic response is included in the Appendix). The message is thus very clear: the high-field slope of the $m(H)$ of MAO contains diamagnetic and paramagnetic contributions that are temperature and sample dependent and thus cannot be safely used to subtract the substrate contribution from the raw data of measured film/substrate samples.

When the complete $m(H)$ loop of a MAO substrate is available, the corresponding raw $m(H)$ data can be subtracted from that of the NFO//MAO film (grown on a substrate of the very same batch) to obtain the magnetization of the NFO film. This is shown in Fig. 2(a), where the raw data at 5 K of NFO//MAO and of the MAO substrate have been subtracted to obtain the
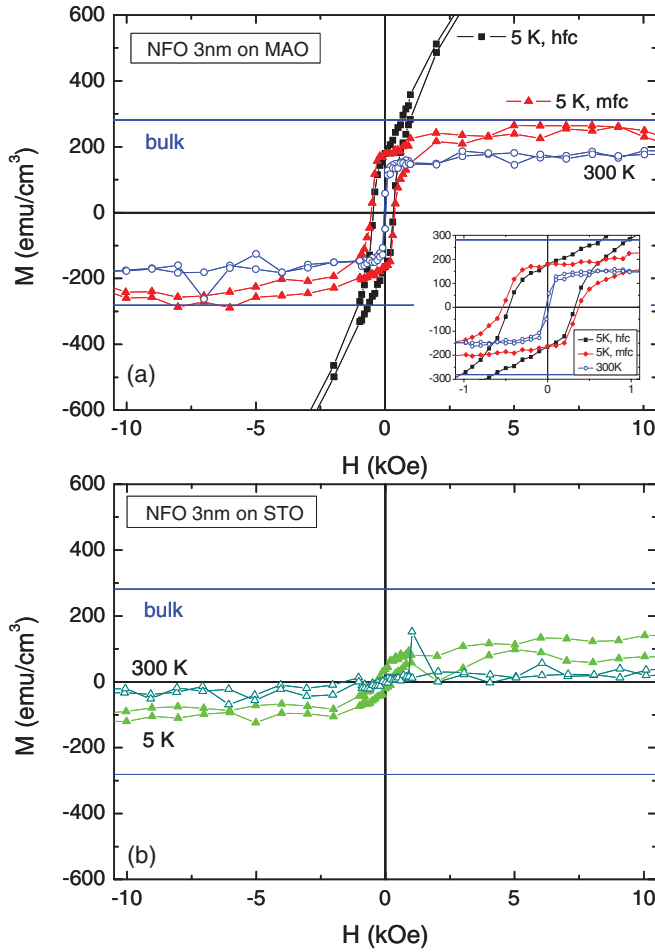
FIG. 3. (Color online) (a) $M(H)$ data for a 3 nm thin NFO layer on MAO after linear subtraction of the high-field slope (hfc) (black squares) and midfield slope (mfc) (red triangles), respectively. Inset: zoom of low-field region, showing the strongly reduced coercive field at 300 K. (b) $M(H)$ data for a 3 nm thin NFO layer on STO after subtracting the high-field slope.
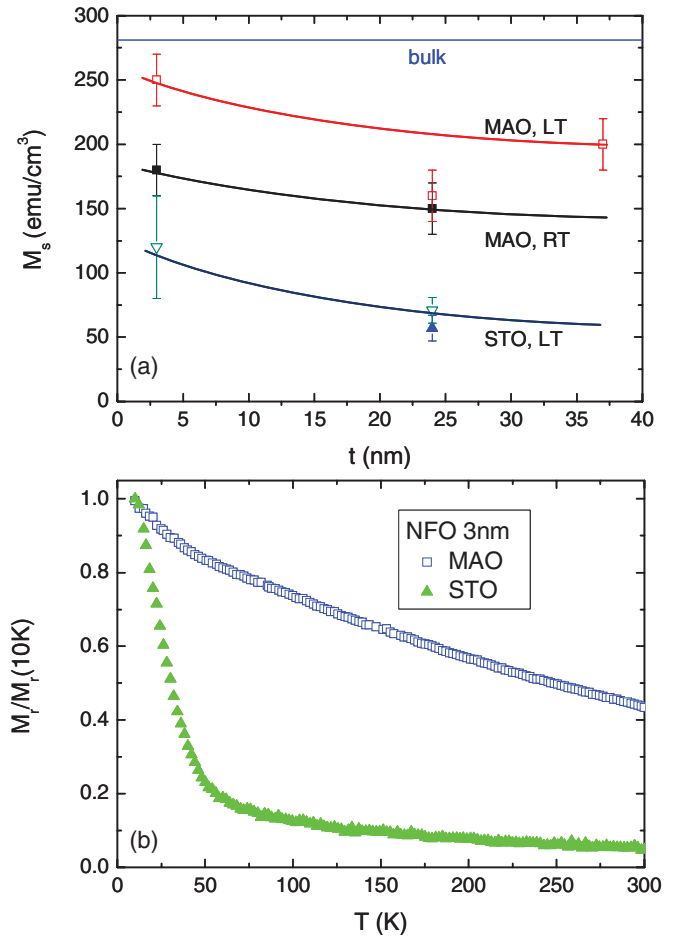
FIG. 4. (Color online) (a) Collected values of saturation magnetization for various samples at different temperatures (LT = 5 or 10 K; RT = 300 K). Lines are guides to the eye. (b) Normalized remanent magnetization of 3 nm NFO layers as function of temperature, obtained after magnetizing by a 50 kOe field at 10 K.

$M(H, 5$ K$)$ curve [open squares, Fig. 2(a)]. One notices that the agreement with data of the bulk NFO powder (open circles) is excellent. This observation confirms that the enhanced saturation magnetization, which one could infer from data obtained using the standard high-field correction [triangles, squares and crosses in Fig. 2(a)], is a spurious effect due to substrate correction. As in this case the spurious contribution is paramagnetic, its influence is strongly temperature dependent and dominates at low temperatures, as can be seen in Fig. 2(a) and also by comparing Figs. 1(b) and 1(c).

Naturally, spurious contributions become increasingly more relevant for thinner films. In Figs. 3(a) and 3(b), we show the $M(H)$ data of the thinnest NFO (3 nm) films grown on MAO and STO, obtained from the raw data of Fig. 1(a) after subtraction of different linear slopes, corresponding to a diamagnetic signal of the substrates. In Fig. 3(a) it can be seen that for NFO//MAO the commonly used linear subtraction of the high-field slope [high-field correction (hfc)] (black squares) leads to high magnetization values (about 10 times the bulk NFO value at 70 kOe). When raw $m(H)$ data of the

identical substrate are not available, substrate correction is not reliable. In this situation, a suitable approach could be to use a linear correction forcing the $M(H)$ data in the range between 5 and 10 kOe to be flat.[14] This mid-field correction (mfc) leads to magnetization values [red triangles in Fig. 3(b)] that agree reasonably well with data from the measurement performed at 300 K (blue open circles). On the STO substrate, there are clear differences between the measurements at low and high temperatures [see Fig. 3(b) for $M(H)$ of NFO(3 nm)//STO after correcting for the high field slope], which will be discussed further below.

In summary, we conclude that our ultrathin NFO (3–37 nm) films grown on either MAO or STO do not exhibit an anomalous enhanced magnetization at any explored temperature but a reduced magnetization when compared to bulk [see Fig. 4(a)]. Paramagnetic contributions from MAO substrates may mask the actual magnetization of the films if not properly corrected.

The next issue to be addressed is the systematic observation of a smaller magnetization of NFO films grown on STO when compared to those grown on MAO. From studies of the magnetic and transport properties of MBE grown

Fe_3O_4 thin films on MgO (see Ref. 5) it was proposed that APBs are formed, which may have a double effect; on one side, its antiferromagnetic nature leads to a reduction of the overall magnetization and, on the other side, they may magnetically uncouple neighbouring ferrimagnetic crystallites thus promoting an SP behavior. Under such circumstances the remanent magnetization (M_r) of the films may rapidly shrink when increasing temperature. While for the thicker films (>24 nm) we did not observe such effect on either substrate, for the thinner films, indeed, a strong decrease of M_r as a function of temperature is found [see Fig. 4(b)]; in particular for NFO (3 nm)//STO, a sharp decay of remanence is observed until 50 K, where it reduces to only about 10% of its value at 10 K, reaching a value at the resolution limit of our SQUID measurement. This behavior is characteristic of superparamagnetism. In contrast, the NFO (3 nm)//MAO remains ferrimagnetic until room temperature, although, as expected for an ultrathin film, its remanence [see Fig. 4(b)] and coercivity [inset of Fig. 3(a)] gradually lower with increasing temperature.

Thus we conclude that (i) ultrathin NFO films on MAO display a magnetization close to, but smaller than, bulk value, and (ii) ultrathin films on STO clearly display an even smaller magnetization and signatures of superparamagnetism.

B. Microstructural characterization

In agreement with XRD data, TEM diffraction patterns obtained along the [100] zone axis on 3 nm thick NFO layers grown on MAO substrate show no visible splitting of spots corresponding to the in-plane lattice constant, indicating that NFO grows fully in-plane strained on MAO. On the other hand, a splitting between the in-plane $(020)_{STO}$ and $(040)_{NFO}$ reflections (and the out-of-plane $(002)_{STO}$ and $(004)_{NFO}$ reflections, respectively) is observed, implying that the NFO layer is nearly fully relaxed on the STO substrate.
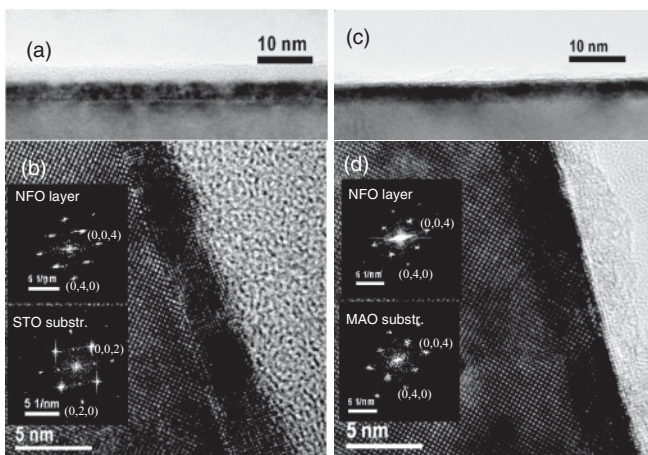

FIG. 5. (a) General view of the NFO(3 nm)//(001)STO sample in cross section geometry observed along the [100] zone axis. (b) Detailed view in HRTEM of the sample. The NFO layer on STO exhibits island growth, resulting in a rougher surface as seen in (a) when compared to (c) and (d) images of the NFO(3 nm)//(001)MAO counterpart, showing a flat free surface and more homogeneous growth of the NFO layer. The insets show the fast Fourier transform (FFT) of the layer and the substrate.
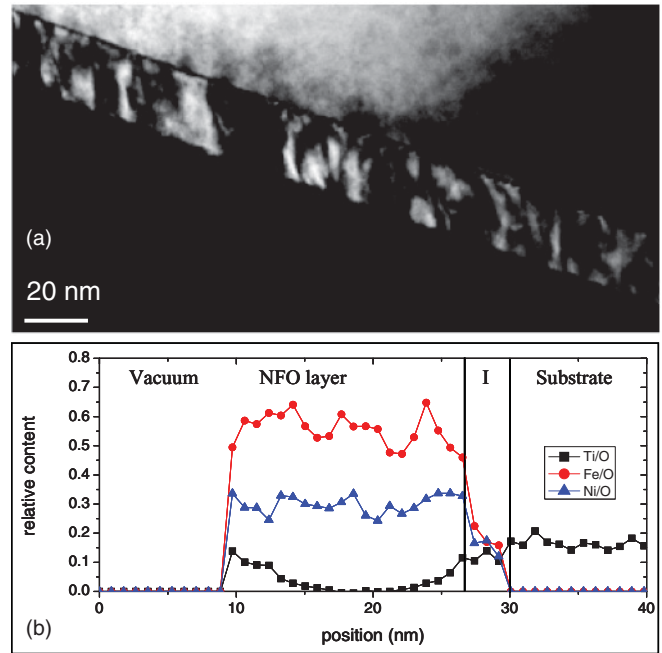

FIG. 6. (Color online) (a) TEM cross-section dark field image of NFO (24 nm)//STO in two-beam condition close to the [100] zone axis using the (022) diffracted beam. Lines of dark contrast through the whole film thickness are visible. (b) Relative composition vs position of NFO(24 nm)//STO determined by EELS, scanning across the NFO-STO interface. The relative content for each indicated element was normalized to the O signal. Regions of different relative compositions are discussed in the text.

In order to disclose the microstructural reasons for the reduced magnetization and SP of the NFO films, HREM and EELS analyses of the samples were performed. HREM images of cross sections of the thinnest NFO films (3 nm) on MAO and STO are shown in Fig. 5. It can be appreciated in Figs. 5(a) and 5(b) that the NFO//STO sample surface is relatively rough suggesting a three-dimensional (3D) growth mechanism. Indeed, detailed inspection of Fig. 5(b) reveals the presence of areas with well-defined contrast, indicating the presence of 3D crystallites and thus 3D growth. The corresponding images obtained of NFO//MAO films [see Figs. 5(c) and 5(d)] show that the NFO film surface is more smooth and there are no visible grains. The presence of 3D islands in the film is relevant as its coalescence may lead to a magnetic frustration similar to APBs in Fe_3O_4. TEM planar views of our 3 nm NFO did not reveal contrast features as those used in Refs. 9 and 15 to identify APBs, and so we may conclude that in this case, 3D islands play a similar role as APBs in decoupling the magnetic response of the crystallites. However, in dark-field HREM cross-section images [see Fig. 6(a)] of NFO(24 nm)//STO, that were obtained in two-beam conditions close to the [100] axis and using the (022) diffracted beam, regions of clear dark-bright contrast can be seen, which could correspond to APBs. Both APBs and the 3D growth may have a similar, detrimental impact on the magnetic coupling within the film. Observation of APBs in thicker NFO films (>200 nm) on STO has been recently reported[16].

A second possible explanation for the reduced magnetization and weak magnetic coupling of NFO films grown on STO was found through the analysis of EELS data recorded across the NFO/STO interface of the same sample. The relative (Ni, Fe, and Ti) compositional profile in Fig. 6(b) (normalized to the local O signal) shows two extended regions of roughly constant Ni and Fe contents and O (not shown), corresponding to the NFO film and STO substrate. These regions are separated by an interface layer (I) about 2–3 nm wide with intermediate contents of all quantified constituents. Such behavior most likely arises simply from the surface roughness although some STO-NFO intermixing can not be excluded. But more importantly, data in Fig. 6(b) demonstrate that Ti is diffusing into the NFO film. It is remarkable that at the upper film surface (at ca. x = 10 nm) a significant Ti content is found, providing clear evidence for Ti diffusion from the STO substrate into and through the NFO layer. Compositional mapping by EELS in cross-section views (not shown here) suggests that Ti interdiffusion occurs mainly through the grain boundaries.

IV. CONCLUSIONS

In summary, we found that ultrathin $NiFe_2O_4$ epitaxial films on MAO display bulklike behavior without evidences of anomalously increased magnetization. The magnetic properties of ultrathin films grown on STO are remarkably different, showing an SP response at temperatures as low as 50 K. This magnetic characteristic is probably related to the observed 3D-island growth and accompanying APBs formation of the spinel nuclei on the poorly matched perovskite substrate. Both the structural difference and the unit cell mismatch between the STO perovskite and the growing NFO spinel should produce a large interfacial energy favoring a Volmer-Weber 3D growth, and subsequently, a magnetic decoupling and so a SP response. Further studies are needed to evaluate the influence of Ti interdiffusion from the STO substrate on the magnetization. These findings may have important implications for spintronic devices based on epitaxial heterostructures involving spinels and perovskite-based oxides. Indeed, one could anticipate that any magnetic contrast or distinctive resistive response under magnetic field or at remanence in tunnel structures based on stacks of these dissimilar oxides should necessarily give a poor response if the spinel layer is SP. To what extent the results reported here are the ultimate reasons for the somewhat better results reported for spinel-based spin filters using magnetite[17] or $\gamma-Al_2O_3$ (see Refs. 2 and 18) (spinel structure) than manganites[11] or $SrRuO_3$ (see Ref. 19) (both with perovskite structure) remains to be confirmed.

APPENDIX: MAGNETIZATION OF THE $MgAl_2O_4$ SUBSTRATE

The field-dependent magnetic moment of the bare MAO substrate shown in Fig. 2(b) was fitted using a superposition of a diamagnetic and a paramagnetic contribution:[20]

$$m(H) = \chi_{DM} H \ + \ N \ g J \mu_B B_J(x),$$

with $x = g J \mu_B \mu_0 H / (k_B T)$ and B_J the Brillouin function and $g = 2$. Here, N is the impurity concentration with a total angular momentum J, χ_{DM} is the diamagnetic susceptibility, and H is the magnetic field intensity. Using the three free parameters (N, J, and χ_{DM}) the agreement of the fit [solid red line in Fig. 2(b)] with experimental data is excellent (goodness of the fit $R > 0.99995$). However, only moderately poorer fits can be obtained by using slightly different values of χ_{DM} as summarized in Fig. 7. In Fig. 7, open circles and solid triangles are the fitted values for J (left scale) and $N J(J + 1)$ (right scale) as a function of the χ_{DM} contribution. Squares indicate the fit quality (R), which in this range is always above $R = 0.997$. The best fit is obtained for $J \approx 3.4$; this value is larger than what would be expected for a single transition-metal ionlike Fe^{3+} impurities thus suggesting either the existence of some clustering or the presence of larger moment impurities, such as rare-earth ions, in MAO. The concentration of impurities N is, as expected, very tiny, in the order of $10^{16}/cm^3$, that is below one part per million (ppm).

The measured temperature-dependent magnetic moment $m(T)$ curve at 1 kOe [bottom inset of Fig. 2(b)] has also been fitted by using a superposition of a Curie law and a temperature-independent diamagnetic susceptibility χ_{DM}:

$$m/H = N J(J + 1) g^2 \mu_B^2/(3 k_B T) + \chi_{DM}.$$

The linear fit of $1/m$ versus T has only two free parameters χ_{DM} and $NJ(J+1)$ and best fit parameters are indicated by a star in Fig. 7. While the result for $N J(J + 1)$ agrees very well with the value for the best fit of $m(H)$ described above, the diamagnetic susceptibility χ_{DM} is only slightly
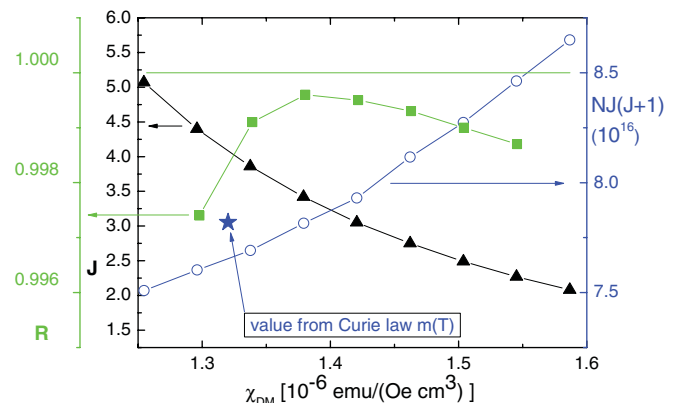

FIG. 7. (Color online) Summary of fit results for the magnetization of the MAO substrate [see Fig. 2(b)] for different diamagnetic corrections χ_{DM} (x axis) as described in Appendix: fit parameters J (black triangles, left scale) and $N J(J + 1)$ (open blue circles, right scale) as well as the fit quality R are shown (green squares, second left scale). The blue star indicates the independent fit result of the $m(T)$ data (right scale) for $N J(J + 1)$ and χ_{DM}.

different from the one obtained for the best fit of $m(H)$. These results are consistent and give compelling evidence for a paramagnetic contribution to the otherwise diamagnetic MAO substrate.

[1] U. Lüders, A. Barthélémy, M. Bibes, K. Bouzehouane, S. Fusil, E. Jacquet, J. P. Contour, J. F. Bobo, J. Fontcuberta, and A. Fert, Adv. Mater. **18**, 1733 (2006).

[2] A. V. Ramos, M.-J. Guittet, J.-B. Moussy, R. Mattana, C. Deranlot, F. Petroff, and C. Gatel, Appl. Phys. Lett. **91**, 122107 (2007).

[3] Y. K. Takahashi, S. Kasai, T. Furubayashi, S. Mitani, K. Inomata, and K. Hono, Appl. Phys. Lett. **96**, 072512 (2010).

[4] L. Néel, Ann. Physik **3**, 137 (1948).

[5] S. K. Arora, H. C. Wu, R. J. Choudhary, I. V. Shvets, O. N. Mryasov, H. Yao, and W. Y. Ching, Phys. Rev. B **77**, 134443 (2008).

[6] U. Lüders, M. Bibes, J. F. Bobo, M. Cantoni, R. Bertacco, and J. Fontcuberta, Phys. Rev. B **71**, 134419 (2005).

[7] R. H. Kodama, A. E. Berkowitz, E. J. Mcniff, and S. Foner, Phys. Rev. Lett. **77**, 394 (1996).

[8] F. C. Voogt, T. T. M. Palstra, L. Niesen, O. C. Rogojanu, M. A. James, and T. Hibma, Phys. Rev. B **57**, R8107 (1998).

[9] W. Erenstein, T. Hibma, and S. Celotto, Phys. Rev B **70**, 184404 (2004).

[10] J. Orna, P. A. Algarabel, L. Morellón, J. A. Pardo, J. M. de Teresa, R. López Antón, F. Bartolomé, L. M. García, J. Bartolomé, J. C. Cezar, and A. Wildes, Phys. Rev. B **81**, 144420 (2010).

[11] U. Lüders, M. Bibes, K. Bouzehouane, E. Jacquet, J.-P. Contour, S. Fusil, J.-F. Bobo, J. Fontcuberta, A. Barthélémy, and A. Fert, Appl. Phys. Lett. **88**, 082505 (2006).

[12] J. S. Moodera, T. S. Santos, T. Nagahama, J. Phys. Condens. Matter **19**, 165202 (2007).

[13] F. Rigato, S. Estradé, J. Arbiol, F. Peiró, U. Lüders, X. Martí, F. Sanchéz, and J. Fontcuberta, Mater. Sci. Eng. B **144**, 43 (2007).

[14] Performing the same *ad-hoc* correction for the data in Fig. 2(a) showed excellent agreement in the low and midfield ranges between the corrected $M(H)$ curve and the $M(H)$ curve obtained by subtracting the MAO substrate. However, this procedure relies on the fact that the ferrimagnetic film is already in or close to saturation in the relevant field range (5–10 kOe).

[15] S. Celotto, W. Eerenstein, and T. Hibma, Eur. Phys. J. B **36**, 271 (2003).

[16] R. Datta, S. Kanuri, S. V. Karthik, D. Mazumdar, J. X. Ma, and A. Gupta, Appl. Phys. Lett. **97**, 071907 (2010).

[17] M. G. Chapline and S. X. Wang, Phys. Rev. B **74**, 014418 (2006).

[18] A. V. Ramos, T. S. Santos, G. X. Miao, M.-J. Guittet, J.-B. Moussy, and J. S. Moodera, Phys. Rev. B **78**, 180402(R) (2008).

[19] F. Rigato, S. Piano, M. Foerster, F. Giubileo, A. M. Cucolo, and J. Fontcuberta, Phys. Rev B **81**, 174415 (2010).

[20] C. Kittel, *Introduction to solid state physics*, 7th ed. (Wiley, New York, 1996).